Solution-Processed Ambipolar Organic Thin-Film Transistors by Blending p- and n-Type Semiconductors: Solid Solution versus Microphase Separation

ARTICLE *in* ACS APPLIED MATERIALS & INTERFACES · APRIL 2015

Impact Factor: 6.72 · DOI: 10.1021/acsami.5b01172 · Source: PubMed

8 AUTHORS, INCLUDING:

Xiaomin Xu
The Chinese University of Hong Kong
12 PUBLICATIONS **192** CITATIONS
SEE PROFILE

Xuejin Yang
The Chinese University of Hong Kong
3 PUBLICATIONS **10** CITATIONS
SEE PROFILE

Stephen V Kershaw
City University of Hong Kong
72 PUBLICATIONS **1,782** CITATIONS
SEE PROFILE

Qian Miao
The Chinese University of Hong Kong
73 PUBLICATIONS **1,913** CITATIONS
SEE PROFILE

ACS APPLIED MATERIALS & INTERFACES

Forum Article

www.acsami.org

Solution-Processed Ambipolar Organic Thin-Film Transistors by Blending p- and n-Type Semiconductors: Solid Solution versus Microphase Separation

Xiaomin Xu,[†] Ting Xiao,[‡] Xiao Gu,[†] Xuejin Yang,[†] Stephen V. Kershaw,[§] Ni Zhao,[‡] Jianbin Xu,[‡] and Qian Miao*[,†,∥]

[†]Department of Chemistry, [‡]Department of Electronic Engineering, and [∥]Center of Novel Functional Molecules, The Chinese University of Hong Kong, Shatin, New Territories, Hong Kong, China

[§]Department of Physics and Materials Science and Centre for Functional Photonics (CFP), City University of Hong Kong, Kowloon, Hong Kong, China

Supporting Information

ABSTRACT: Here, we report solid solution of p- and n-type organic semiconductors as a new type of p−n blend for solution-processed ambipolar organic thin film transistors (OTFTs). This study compares the solid-solution films of silylethynylated tetraazapentacene **1** (acceptor) and silylethynylated pentacene **2** (donor) with the microphase-separated films of **1** and **3**, a heptagon-embedded analogue of **2**. It is found that the solid solutions of $(\mathbf{1})_x(\mathbf{2})_{1-x}$ function as ambipolar semiconductors, whose hole and electron mobilities are tunable by varying the ratio of **1** and **2** in the solid solution. The OTFTs of $(\mathbf{1})_{0.5}(\mathbf{2})_{0.5}$ exhibit relatively balanced hole and electron mobilities comparable to the highest values as reported for ambipolar OTFTs of stoichiometric donor−acceptor cocrystals and microphase-separated p-n bulk heterojunctions. The solid solution of $(\mathbf{1})_{0.5}(\mathbf{2})_{0.5}$ and the microphase-separated blend of **1**:**3** (0.5:0.5) in OTFTs exhibit different responses to light in terms of absorption and photoeffect of OTFTs because the donor and acceptor are mixed at molecular level with $\pi-\pi$ stacking in the solid solution.

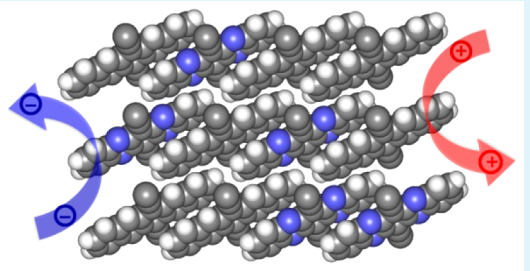

KEYWORDS: *organic semiconductors, solid solution, microphase separation, organic thin film transistors, ambipolar*

INTRODUCTION

Ambipolar organic thin film transistors (OTFTs) with balanced charge carriers (electrons and holes) can provide both n- and p-channel performance and thus enable complementary integrated circuits without advanced patterning techniques.[1] Ambipolar charge transport in OTFTs can be realized by either a single-component ambipolar semiconductor or a combination of two unipolar (p- and n-type) semiconductors. Achieving balanced and high hole and electron mobilities with a single-component organic semiconductor is difficult[2] because of the problem of unequal charge carrier injection into the semiconductor. The reported high-performance ambipolar organic semiconductors are dominated by narrow-band-gap polymers.[3] To achieve ambipolar charge transport in OTFTs, one p-type and one n-type semiconductors can be combined in the form of bilayer or blend. Most of the reported p−n semiconductor bilayers in ambipolar OTFTs were fabricated by vacuum deposition[4,5] because solution processing of p−n bilayers[6,7] are challenging because of the need for finding an orthogonal solvent for the deposition of the second layer.[1] In contrast, a blend of p- and n-type organic semiconductors can be fabricated by either processing a mixed solution or by codeposition of two components under vacuum, leading to different microstructures. The most common p−n blend is a bulk heterojunction,[8−14] which is an interpenetrating network of a p-type semiconductor and an n-type semiconductor with microphase separation, and is also widely used as the active layer in organic photovoltaic solar cells. Another type of blend is a stoichiometric complex of p-type and n-type organic semiconductors, where the two components cocrystallize in the same lattice.[15−20] In such cocrystals, the p-type and n-type semiconductors usually have a ratio of 1:1 and often exhibit an alternative arrangement in π-stacks. Unlike the bulk heterojunction, where the interfaces between p- and n-type semiconductors are greatly affected by processing, the stoichiometric cocrystal is regarded as a "molecular level heterojunction",[17] where the interfaces between p- and n-type semiconductor molecules are defined by the crystal structures.

Here, we report solid solution of p- and n-type organic semiconductors as a new type of p−n blend for solution-processed ambipolar OTFTs. Solid solution is "a solid mixture

Special Issue: Advances towards Electronic Applications in Organic Materials

Received: February 7, 2015
Accepted: April 13, 2015

DOI: 10.1021/acsami.5b01172
ACS Appl. Mater. Interfaces XXXX, XXX, XXX−XXX

of one or more compounds within a "solvent" of another crystalline compound".[21] Therefore, solid solution of p- and n-type organic semiconductors is conceptually different from either microphase-separated p−n heterojunctions or stoichiometric donor−acceptor complexes.[22] To better understand this difference, in this study, the p−n solid solution was compared with a microphase-separated p−n heterojunction of structurally related molecules. Solid solutions of p-type and n-type organic semiconductors are almost unexplored. To the best of our knowledge, vacuum codeposited copper phthalocyanine (CuPc) and copper perfluorophthalocyanine (F_{16}CuPc) were reported as crystal "phases with different intermixing ratio between CuPc and F_{16}CuPc molecules", but were not formally recognized as solid solutions.[23] In close relation to the p−n solid solutions, we recently reported solid solutions of silylethynylated tetracene and diazatetracene, which contained one insulating component and one n-type semiconductor component.[24]

Three solution-processed unipolar semiconductors (**1**−**3**) with closely related structures as shown in Figure 1 were

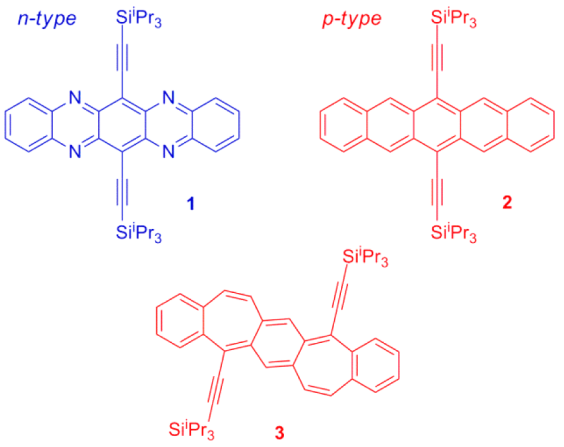

Figure 1. Molecular structures of the silylethynylated tetraazapentacene **1**, pentacene **2**, and heptagon-embedded pentacene **3**.

selected for this study. Among them, silylethynylated tetraazapentacene **1** is an n-type semiconductor,[25,26] which exhibits field effect mobility of up to 5.0 $cm^2 V^{-1} s^{-1}$ in solution processed OTFTs.[27,28] Silylethynylated pentacene **2**[29] is a widely studied solution-processed p-type semiconductor exhibiting field effect mobility higher than 1.0 $cm^2 V^{-1} s^{-1}$ in unstrained films,[30,31] and of up to 4.6 $cm^2 V^{-1} s^{-1}$ in strained films.[32] Compound **3**, a heptagon-embedded analogoue of **2**, is a p-type semiconductor recently developed by us exhibiting field effect mobility close to 1.0 $cm^2 V^{-1} s^{-1}$ in solution-processed OTFTs.[33] With nitrogen atoms replacing carbon atoms in the pentacene framework, **1** has a molecular shape almost identical to that of **2**. Moreover, **1** and **2** share the same two-dimensional π-stacking with very similar crystal lattices because the bulky triisopropylsilyl substituents are a determinant of molecular packing. We therefore hypothesized that, similar to phthalocyanines with different central metal cations,[34,35] **1** and **2** are able to intermix to form solid-solution crystals. In contrast, the molecular shape of **3** apparently differs from that of **1** by having two heptagons and two bulky substituting groups at different positions. Moreover, molecules of **3** are packed in one-dimensional π-stacks with a crystal lattice very different to that of **1**. In agreement with this, it was found that cocrystallization of **1** and **2** resulted in solid solutions, whereas crystallization of **1** and **3** under similar conditions resulted in separate single-component crystals. Detailed below is a comparative study on the ambipolar OTFTs containing solid solutions of **1** and **2** and microphase-separated blends of **1** and **3** as the semiconductor layer.

RESULTS AND DISCUSSION

Solid-Solution Crystals. Cocrystals of **1** and **2** were conveniently grown from mixed solutions by slow evaporation of solvents. Shown in Figure 2a is the polarized-light

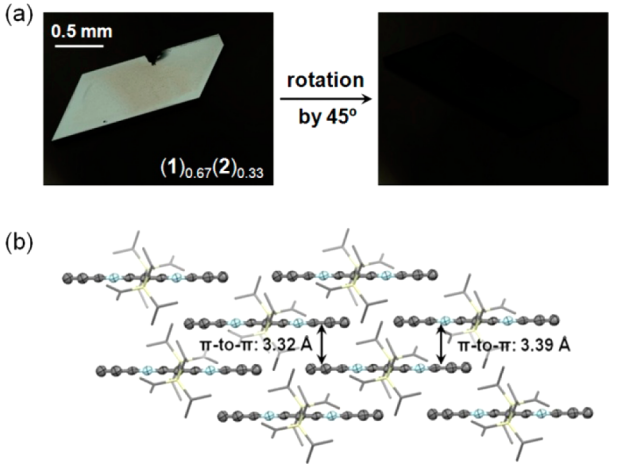

Figure 2. (a) Reflected polarized-light micrographs of the cocrystal. (b) Two-dimensional π-stacking in $(\mathbf{1})_{0.5}(\mathbf{2})_{0.5}$ cocrystal. (Atoms in the tetracyclic backbone are shown as ellipsoids at 50% probability level and silylethynyl substituents are shown as capped sticks, hydrogen atoms are removed for clarification, the light blue atoms contain carbon and nitrogen.)

micrograph for a typical cocrystal of **1** and **2** as grown from solution in ethyl acetate. Rotating the crystal by 45° under cross-polarized light led to extinction, indicating these cocrystals were single crystals.[36] Ratio of the two components in the cocrystals was determined by dissolving the cocrystals in $CDCl_3$ and comparing the ^{1}H NMR spectra integrals of the corresponding peaks.[24] It was found that the ratio varied among crystals obtained from the same solution. For example, the ratio of **1** and **2** in the cocrystals obtained from a 1:1 mixed solution of **1** and **2** varied from 2:1 to 1:2. This is in agreement with solid solutions rather than stoichiometric cocrystals. To show the composition, the cocrystals are presented as $(\mathbf{1})_x(\mathbf{2})_{1-x}$ here. By varying the relative concentrations of two components in the mixed solution, cocrystals of $(\mathbf{1})_x(\mathbf{2})_{1-x}$ with x varied from 0.05 to 0.95 were obtained.

Single cocrystals of $(\mathbf{1})_{0.82}(\mathbf{2})_{0.18}$, $(\mathbf{1})_{0.50}(\mathbf{2})_{0.50}$ and $(\mathbf{1})_{0.23}(\mathbf{2})_{0.77}$ were qualified for X-ray crystallography, and their crystal structures are summarized in Table 1. The crystal structures of these cocrystals contain only one type of molecule having mixed carbon and nitrogen atoms, suggesting a random arrangement of **1** and **2** in the crystal lattice. In comparison to the single-component crystal of either **1**[26] or **2**,[29] the cocrystals of $(\mathbf{1})_x(\mathbf{2})_{1-x}$ exhibit very similar unit cells as summarized in Table 1 and nearly the same two-dimensional π-stacking with brickwork arrangement as shown in Figure 2b. Besides a molecular-level mixing of the two components with random distribution, another possible arrangement of **1** and **2** in the cocrystals is separated distribution of **1** and **2** in a way similar to

DOI: 10.1021/acsami.5b01172
ACS Appl. Mater. Interfaces XXXX, XXX, XXX−XXX

Table 1. Summary of Crystal Structures of 1, 2, 3, and Cocrystals of $(1)_x(2)_{1-x}$

	1[26]	2[29]	3[33]	$(1)_{0.82}(2)_{0.18}$	$(1)_{0.50}(2)_{0.50}$	$(1)_{0.23}(2)_{0.77}$
space group	$P\bar{1}$	$P\bar{1}$	$P\bar{1}$	$P\bar{1}$	$P\bar{1}$	$P\bar{1}$
unit cell lengths (Å)	a = 7.5841	a = 7.565	a = 8.2582	a = 7.5962	a = 7.614	a = 7.7025
	b = 7.612	b = 7.750	b = 8.4593	b = 7.7187	b = 7.647	b = 7.708
	c = 16.8363	c = 16.835	c = 14.615	c = 16.939	c = 16.876	c = 16.958
unit cell angles (deg)	α = 78.981	α = 89.15	α = 87.393	α = 78.487	α = 78.31	α = 78.06
	β = 89.541	β = 78.42	β = 87.145	β = 89.106	β = 88.812	β = 88.605
	γ = 81.90	γ = 83.63	γ = 88.066	γ = 81.261	γ = 82.064	γ = 82.113
cell volume (Å^3)	944.3	960.9	1018.5	961.8	953.0	975.7
R-factor	0.0375	0.0486	0.0580	0.0584	0.0714	0.0547
packing motif	2D brickwork	2D brickwork	1D π-stacking	2D brickwork	2D brickwork	2D brickwork

the microphase separation resulting in mixing of nanometer-sized crystallites of **1** or **2**. The crystal structures of $(1)_x(2)_{1-x}$ themselves do not entirely exclude this possibility because the nitrogen atoms in **1** cannot be distinguished from the carbon atoms in **2** by X-ray crystallography and the unit cells of **1** and **2** are very similar. However, the single-crystal nature of the $(1)_x(2)_{1-x}$ solid solutions suggests such nanometer-scaled phase separation of **1** and **2** is unlikely.

Thin Films of Solid Solutions and Microphase-Separated Blends. To compare solid solutions of p−n semiconductors with the widely studied microphase-separated blends, thin films of $(1)_x(2)_{1-x}$ and microphase-separated blend of **1** and **3** were prepared by a dip coating process, which involved faster solvent evaporation than the growth of single crystals of $(1)_x(2)_{1-x}$ from solution. In relation to the fabrication of ambipolar OTFTs, a high-k dielectric of aluminum oxide and titanium oxide (AlO_y/TiO_x)[37] on silicon was used as the substrate, which was pretreated with a self-assembled monolayer (SAM) of 12-cyclohexyldodecylphosphonic acid (CDPA in Figure 3a) to passivate surface hydroxyl

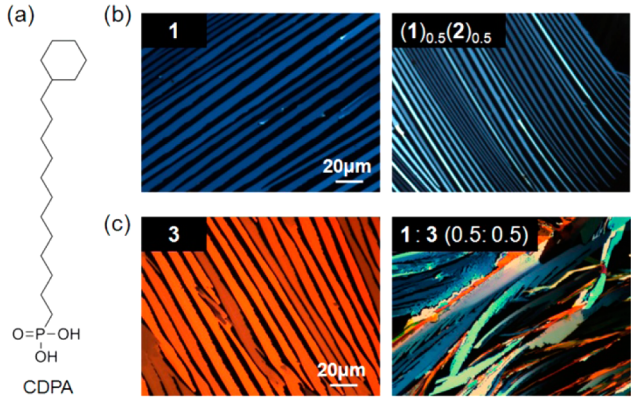

Figure 3. (a) Molecular structure of CDPA, which is used to modify the AlO_y/TiO_x dielectric surface in the solution-processed thin films and OTFTs; (b) reflected polarized-light micrographs for the thin films of neat **1** (left) and solid solution $(1)_{0.5}(2)_{0.5}$ (right); (c) reflected polarized-light micrographs for the films of **3** (left) and **1**:**3** (0.5:0.5) (right).

groups and to maintain sufficient surface energy for good wettability.[28] In order to optimize the conditions for dip coating, different solvents were tested, and a mixed solvent of dichloromethane and acetone (1:1 by volume) was found the best for this process. To prepare blend films with varied ratios of p- and n-type semiconductors, the total concentration of **1** and **2** or **1** and **3** in dichloromethane and acetone (1:1 by volume) was fixed as 2.3 mmol/L and the ratio of the two components varied from 1:6 to 6:1. The substrate was immersed in the solution and then pulled up with a constant speed at 10 μm/s, leading to crystalline blend films containing p- and n-type components with varied ratio. In the following discussion, the microphase-separated blend of **1** and **3** is noted as **1**:**3** (x:1−x) to differ from the solid solution of $(1)_x(2)_{1-x}$. The value of x for the solid-solution and microphase-separated films both refer to those in the solutions used for dip coating.

The dip-coated films of $(1)_{0.5}(2)_{0.5}$ and **1**:**3** (0.5:0.5) were studied in a comparative manner with polarized-light microscopy, X-ray diffraction (XRD), Kelvin probe force microscopy (KPFM) and UV−vis absorption spectroscopy. Figure 3b shows the polarized-light micrograph of a $(1)_{0.5}(2)_{0.5}$ film, which exhibits aligned stripes with homogeneous color similar to those of the neat film of **1**, in agreement with mixing at molecular level in the solid solution. In contrast, the polarized-light micrograph of a **1**:**3** (0.5:0.5) film (Figure 3c) exhibits mixed stripes of varied colors, which are unlike the neat film of either **1** or **3**. Such different appearance can be attributed to phase separation of **1** and **3**. Separate crystallization of **1** and **3** with different speed leads to poor alignment of crystalline fibers as observed.

Figure 4a shows the X-ray diffraction patterns from the films of $(1)_{0.5}(2)_{0.5}$, **1**, and **2**, which are essentially the same because

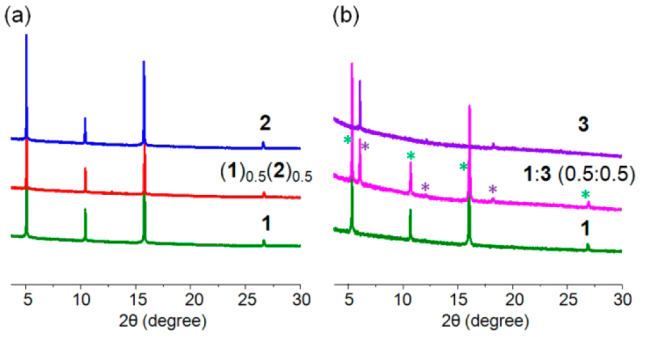

Figure 4. X-ray diffraction patterns from the thin films of (a) **1**, **2**, and $(1)_{0.5}(2)_{0.5}$; (b) **1**, **3**, and **1**:**3** (0.5:0.5).

the crystal lattices of $(1)_{0.5}(2)_{0.5}$ are very close to those of **1** and **2** as shown in Table 1. The film of $(1)_{0.5}(2)_{0.5}$ exhibits four diffraction peaks at 2θ = 5.34° (d spacing of 16.56 Å), 2θ = 10.68° (d spacing of 8.28 Å), 2θ = 16.04° (d spacing of 5.52 Å), and 2θ = 26.88° (d spacing of 3.31 Å). These diffractions correspond to the (001), (002), (003), and (005) diffractions

DOI: 10.1021/acsami.5b01172
ACS Appl. Mater. Interfaces XXXX, XXX, XXX−XXX

derived from the single-crystal structure of $(\mathbf{1})_{0.5}(\mathbf{2})_{0.5}$ cocrystal, indicating a highly ordered film with layered structures. In contrast, the film of **1**:**3** (0.5:0.5) exhibits two sets of X-ray diffraction peaks as marked with green star and purple star in Figure 4b. The peaks marked with green star are the same as those from the neat film of **1**, and correspond to the (001), (002), (003), and (005) diffractions derived from the single-crystal structure of **1**. The peaks marked with purple star are the same as those from the neat film of **3** appearing at $2\theta = 6.07°$ (d spacing of 14.56 Å), $2\theta = 12.13°$ (d spacing of 7.29 Å), and $2\theta = 18.25°$ (d spacing of 4.86 Å). They correspond to the (001), (002) and (003) diffractions derived from the single-crystal structure of **3**. The diffraction patterns of **1**:**3** (0.5:0.5) clearly indicate phase separation, whereas the diffraction patterns of $(\mathbf{1})_{0.5}(\mathbf{2})_{0.5}$ are in agreement with solid solutions but do not entirely exclude the possibility of phase separation because the diffraction peaks from films of **1** and **2** are too close to be distinguished.

As shown in Figure 5, both topography and surface potential of the dip-coated films of $(\mathbf{1})_{0.5}(\mathbf{2})_{0.5}$ and **1**:**3** (0.5:0.5) were

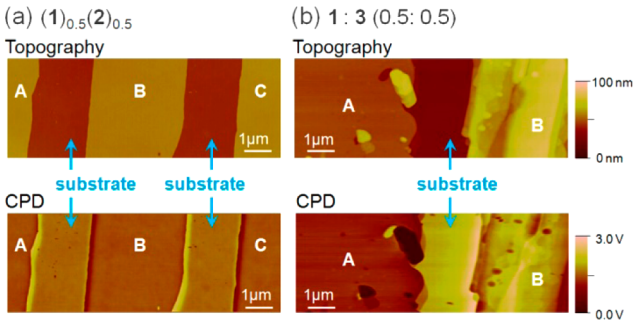

Figure 5. Topography and corresponding contact potential difference (CPD) images for the thin films of (a) $(\mathbf{1})_{0.5}(\mathbf{2})_{0.5}$ and (b) **1**:**3** (0.5:0.5).

mapped with Kelvin probe force microscopy (KPFM), which measures a contact potential difference (CPD) between the sample surface and the tip[38−40] and has been widely used to study microphase-separated p-n heterojunctions.[41−43] The topographical image in Figure 5a reveals that the drop-cast film of $(\mathbf{1})_{0.5}(\mathbf{2})_{0.5}$ is composed of nearly parallel smooth stripes, which are a few micrometers wide and separated by about 2 μm. In the CPD image from the same area, the microstripes (noted as A, B, and C) have nearly the same color. This suggests absence of phase separation at micron scale, in agreement with a solid solution involving molecular level mixing of p- and n-type semiconductors. In contrast, the topographical image in Figure 5b shows that the film of **1**:**3** (0.5:0.5) contains much rougher and less regular stripes. In the CPD image from the same area, the organic domains noted as A and B show apparently different colors suggesting different chemical compositions in the two areas. By comparing the CPD of domains A and B with the CPD of neat films of **1** and **3**, domain A can be assigned to compound **1**, whereas domain B can be assigned to compound **3**.

Figure 6a compares the absorption spectra of **1**, **2**, and $(\mathbf{1})_{0.5}(\mathbf{2})_{0.5}$ in the visible and near-infrared region. It is found that the film of $(\mathbf{1})_{0.5}(\mathbf{2})_{0.5}$ exhibits an extra broad peak as labeled with shadows in the range of 780 to 1046 nm. In the same region, the neat film of **1** has no absorption, whereas the neat film of **2** exhibits a broad absorption shoulder. Therefore,

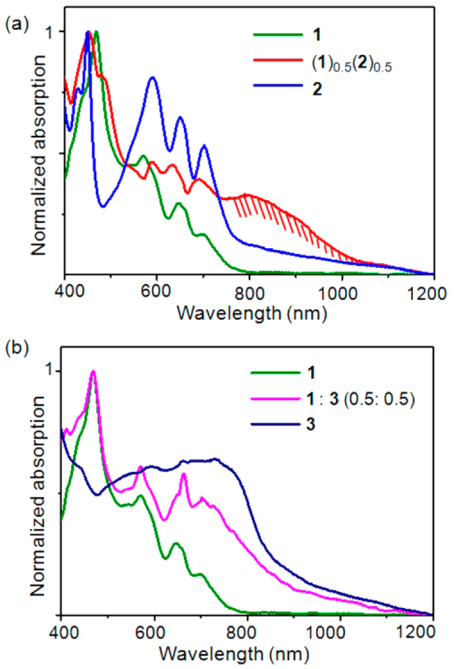

Figure 6. Absorption spectra in the visible and near-infrared region for (a) dip-coated films of **1**, **2**, and $(\mathbf{1})_{0.5}(\mathbf{2})_{0.5}$ and (b) dip-coated films of **1**, **3**, and **1**:**3** (0.5:0.5).

the absorption peak of $(\mathbf{1})_{0.5}(\mathbf{2})_{0.5}$ in the near-infrared region is not due to superposition of the absorption of neat **1** and **2**, but should be attributed to a charge-transfer band due to electronic transition from the highest occupied molecular orbital (HOMO) of **2** to the lowest unoccupied molecular orbital (LUMO) of **1**.[20,44−47] The HOMO energy levels of **1** and **2** are −5.75 and −5.17 eV, respectively, and the LUMO energy levels of **1** and **2** are −4.01 and −3.30 eV, respectively.[26] Therefore, the electronic transition from the HOMO of **2** to the LUMO of **1** corresponds to absorption at 1068 nm (1.16 eV), which is in agreement with the charge transfer band of the $(\mathbf{1})_{0.5}(\mathbf{2})_{0.5}$ solid solution. In contrast, the absorption spectrum of the blend film **1**:**3** (0.5:0.5) appears as a superposition of the spectra of neat **1** and **3** without extra absorption. The presence of charge transfer band in the absorption spectrum of $(\mathbf{1})_{0.5}(\mathbf{2})_{0.5}$ is in agreement with its solid solution nature. The molecules of **1** (acceptor) and **2** (donor) in the solid solution are mixed at molecular level and are closely contacted with a face-to-face π-stacking, which facilitates the interactions between the HOMO of **2** and the LUMO of **1**. On the other hand, the absence of charge transfer band in the absorption spectrum of **1**:**3** (0.5:0.5) is in agreement with microphase separation, which only allows close contacts between donor and acceptor molecules at the interfaces of two types of crystallites.

Combination of the above findings from polarized-light microscopy, XRD, KPFM, and absorption spectroscopy support the conclusion that the film of $(\mathbf{1})_{0.5}(\mathbf{2})_{0.5}$ is a solid solution with mixing at molecular level while the film of **1**:**3** (0.5:0.5) is microphase-separated.

Ambipolar OTFTs. To compare the semiconductor properties of p−n solid solution and microphase-separated blend in OTFTs, thin films of $(\mathbf{1})_x(\mathbf{2})_{1-x}$ and **1**:**3** (x:1−x) were dip-coated on the CDPA-modified AlO_y/TiO_x substrates. In this dip-coating process, the substrate was pulled up with a constant speed from a mixed solution of **1** and **2** or **1** and **3** in dichloromethane and acetone (1:1 by volume). The pulling

DOI: 10.1021/acsami.5b01172
ACS Appl. Mater. Interfaces XXXX, XXX, XXX−XXX

speed was optimized as 1.2 μm/s, which was slower than that used to form thin films shown in Figure 3b to achieve suitable thickness and coverage. The ratio of **1** to **2** or **1** to **3** in the mixed solution was changed from 1:6 to 6:1 so that x in the films of $(\mathbf{1})_x(\mathbf{2})_{1-x}$ and **1**:**3** (x:1−x) varied from 0.14 to 0.86. The device fabrication was completed by depositing a layer of gold on the dip-coated organic films through a shadow mask in vacuum with the direction of channel nearly parallel to the direction of crystalline fibers.

It was found that both the solid-solution films of $(\mathbf{1})_x(\mathbf{2})_{1-x}$ and the microphase-separated films **1**:**3** (x:1−x) generally behaved as ambipolar semiconductors, which were mainly electron-transporting when $x \geq 0.5$ and were mainly hole-transporting when $x < 0.5$. This suggests that the donor−acceptor binary films possess more pathways for electrons than for holes when **1** is the major component and vice versa. As summarized in Figure 7a, when the value of x in $(\mathbf{1})_x(\mathbf{2})_{1-x}$

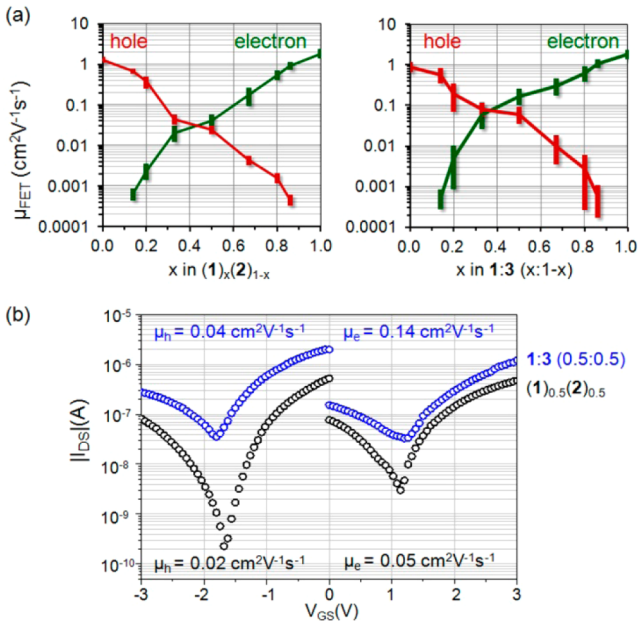

Figure 7. (a) Field-effect mobility (μ_{FET}) for OTFTs of $(\mathbf{1})_x(\mathbf{2})_{1-x}$ (left) and **1**:**3** (x:1−x) (right) as measured from at least four OTFT devices for each composition. (Electron and hole mobilities are shown in red and green, respectively, and the vertical bars represent the standard derivation.) (b) Transfer I−V curves for the OTFTs of $(\mathbf{1})_{0.5}(\mathbf{2})_{0.5}$ (black circles) and **1**:**3** (0.5:0.5) (magenta circles) with an active channel of 1 mm wide and 50 μm long as measured under vacuum.

decreases from 0.86 to 0.14, the hole mobility increases from (4 ± 1) × 10^{-4} cm^2 V^{-1} s^{-1} to 0.7 ± 0.1 cm^2 V^{-1} s^{-1} whereas the electron mobility decreases from 0.9 ± 0.1 cm^2 V^{-1} s^{-1} to (6 ± 1) × 10^{-4} cm^2 V^{-1} s^{-1}. Similarly, when the value of x in **1**:**3** (x:1−x) decreases from 0.86 to 0.14, the hole mobility increases from (6 ± 4) × 10^{-4} cm^2 V^{-1} s^{-1} to 0.6 ± 0.2 cm^2 V^{-1} s^{-1}, whereas the electron mobility decreases from 1.1 ± 0.1 cm^2 V^{-1} s^{-1} to (5 ± 2) × 10^{-4} cm^2 V^{-1} s^{-1}. In comparison to these results, the neat films of **1** exhibited field-effect mobility of 1.8 ± 0.2 cm^2 V^{-1} s^{-1} for electrons while the neat films of **2** and **3** exhibited field effect mobility of 1.3 ± 0.2 cm^{2}V^{-1} s^{-1} and 0.9 ± 0.1 cm^2 V^{-1} s^{-1} for holes, respectively, in control experiments. These results indicate that the ambipolar property of both solid solution and microphase-separated blend is tunable by varying the ratio of p- and n-type components.

The ambipolar charge transport in the solid solutions of $(\mathbf{1})_x(\mathbf{2})_{1-x}$ and the microphase-separated films of **1**:**3** (x:1−x) indicates existence of pathways for transport of both holes and electrons in the two types of films. Unlike the films of **1**:**3** (x:1−x) containing microphase-separated domains of **1** and **3** for transport of electrons and holes, respectively, the solid solutions of $(\mathbf{1})_x(\mathbf{2})_{1-x}$ is homogeneous having one pathway for transport of both electrons and holes due to mixing of **1** and **2** at molecular level. Therefore, the ambipolar transport in $(\mathbf{1})_x(\mathbf{2})_{1-x}$ involves two types of charge transport. One is favorable transport between molecules of the same component, namely electron transport between molecules of **1** and hole transport between molecules of **2**. The other is unfavorable transport between molecules of two different components involving removal of electron from the HOMO of **1** or injection of electron into the LUMO of **2**. These two electronic processes are unfavorable but can still occur because the HOMO of **1** (−5.75 eV) is not too low and the LUMO of **2** (−3.30 eV) is not too high. In fact, ambipolar transport in single crystals of **2** was observed showing electron mobility smaller than hole mobility by 2 orders of magnitude.[48] Moreover, the microphase-separated films of **1**:**3** (x:1−x) exhibited higher electron and hole mobilities than the solid solution films of $(\mathbf{1})_x(\mathbf{2})_{1-x}$ suggesting that the bicontinuous pathways in the microphase-separated films allow more efficient transport of both electrons and holes than the homogeneous solid solutions.

Figure 7b shows typical transfer curves for OTFTs of $(\mathbf{1})_{0.5}(\mathbf{2})_{0.5}$ and **1**:**3** (0.5:0.5) as measured in a vacuum and under ambient light. The field effect mobilities extracted from the transfer curves of $(\mathbf{1})_{0.5}(\mathbf{2})_{0.5}$ is 0.02 cm^2 V^{-1} s^{-1} for hole and 0.05 cm^2 V^{-1} s^{-1} for electron, and the mobilities extracted from the transfer curves of **1**:**3** (0.5:0.5) is 0.04 cm^2 V^{-1} s^{-1} for hole and 0.14 cm^2 V^{-1} s^{-1} for electron. The relatively balanced hole and electron mobilities of $(\mathbf{1})_{0.5}(\mathbf{2})_{0.5}$ are comparable to the highest values of the reported ambipolar OTFTs of stoichiometric donor−acceptor cocrystals,[15−20] microphase-separated p−n bulk heterojunctions[8−14] or epitaxial p−n junctions.[49] Moreover, the transistor of $(\mathbf{1})_{0.5}(\mathbf{2})_{0.5}$ exhibits off currents lower than that of **1**:**3** (0.5:0.5) by 1−2 orders of magnitude. This can be attributed to a doping effect at the interfaces between donor and acceptor domains in the microphase separated films of **1**:**3** (0.5:0.5).[50]

When tested under light and dark conditions, the OTFTs of $(\mathbf{1})_{0.5}(\mathbf{2})_{0.5}$ solid solution exhibited almost the same I−V characteristics without any apparent photo effects. In contrast, the OTFTs of **1**:**3** (0.5:0.5), similar to the reported ambipolar OTFTs of microphase-separated p−n blends,[13,14] exhibited larger drain currents under light than in the dark. Figure 8a compares transfer I−V curves of the OTFT of $(\mathbf{1})_{0.5}(\mathbf{2})_{0.5}$ as tested in the dark and under a red light with an intensity of 3.0 mW/cm^2 and a peak wavelength at 627 nm.[51] The absence of photo effect in the OTFTs of $(\mathbf{1})_{0.5}(\mathbf{2})_{0.5}$ is likely due to fast recombination of photoinduced electrons and holes in the solid solutions, where donor and acceptor molecules are intimately contacted with π−π stacking. Similarly, most of the ambipolar transistors of stoichiometric donor−acceptor cocrystals are not reported to exhibit photo effects, except a very small photocurrent observed from the stoichiometric cocrystals of a sulfur-bridged annulene and C_{70}.[20] Figure 8b compares transfer I−V curves of the OTFT of **1**:**3** (0.5:0.5) as tested in the dark and under the same red light, showing a ratio of photocurrent and dark-current (I_{ph}/I_{dark}) as high as 1 order of magnitude.

DOI: 10.1021/acsami.5b01172
ACS Appl. Mater. Interfaces XXXX, XXX, XXX−XXX

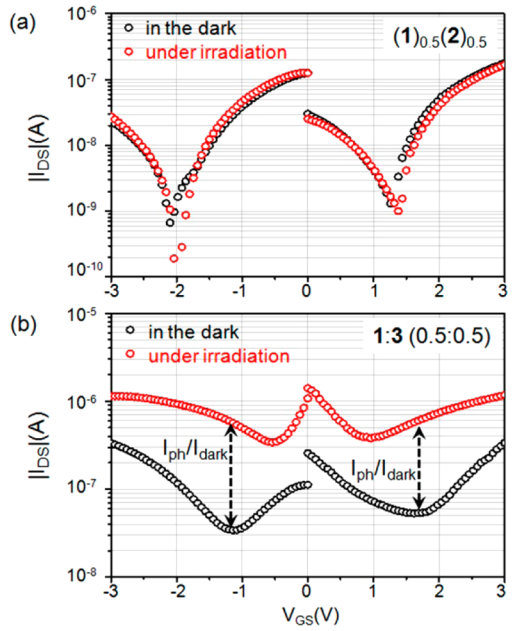

Figure 8. Transfer $I-V$ curves for the OTFTs of (a) $(\mathbf{1})_{0.5}(\mathbf{2})_{0.5}$ and (b) **1:3** (0.5:0.5) as tested at a drain voltage of 3 V for n-channel and −3 V for p-channel in the dark and under red light (627 nm, 3.0 mW/cm^2). The active channels have channel width of W = 1 mm and channel length of L = 150 μm.

This photo effect is associated with a shift of threshold voltage by about 2 V as shown in Figure S4 (Supporting Information), because of photoinduced charge carriers. Although photoinduced charge separation can only occur at the interfaces between crystallites of **1** and **3**, the separated electrons and holes can be separately transported through the segregated domains of **1** and **3**, respectively, leading to enhanced photocurrent.

CONCLUSIONS

In summary, we have demonstrated that tetraazapentacene **1** (acceptor) and pentacene **2** (donor) can form solid-solution crystals, which are conceptually different from either microphase-separated donor−acceptor heterojunctions or stoichiometric donor−acceptor complexes. Dip-coated films of $(\mathbf{1})_{0.5}(\mathbf{2})_{0.5}$ solid solutions were characterized with varied techniques in comparison to microphase-separated films of **1:3** (0.5:0.5). It was found that $(\mathbf{1})_x(\mathbf{2})_{1-x}$ solid solutions functioned as ambipolar semiconductors, whose hole and electron mobilities could be conveniently tuned by varying the ratio of **1** and **2** in the solid solution. The OTFTs of $(\mathbf{1})_{0.5}(\mathbf{2})_{0.5}$ exhibited hole and electron mobilities of $(2.0 \pm 0.1) \times 10^{-2}$ and $(5.0 \pm 0.8) \times 10^{-2}$ cm^2 V^{-1} s^{-1}, respectively, which are comparable to the highest values as reported for ambipolar field effect transistors of stoichiometric donor−acceptor cocrystals and microphase-separated p-n bulk heterojunctions. The films of $(\mathbf{1})_{0.5}(\mathbf{2})_{0.5}$ and **1:3** (0.5:0.5) differ in their response to light in terms of absorption and photoeffect of OTFTs because, unlike the microphase-separated blends, the solid solutions involve mixing of donor and acceptor at molecular level with $\pi-\pi$ stacking.

ASSOCIATED CONTENT

Supporting Information

Details for the fabrication and characterization of thin films and OTFTs, and crystallographic information files (CIF) for the single crystals of solid solutions. This material is available free of charge via the Internet at http://pubs.acs.org.

AUTHOR INFORMATION

Corresponding Author

*E-mail: miaoqian@cuhk.edu.hk.

Notes

The authors declare no competing financial interest.

ACKNOWLEDGMENTS

We thank Prof. Thomas C. W. Mak for helpful discussion and Ms. Hoi Shan Chan for single-crystal crystallography. This work was supported by the Research Grants Council of Hong Kong (project number: GRF402613).

DEDICATION

Dedicated to Prof. Fred Wudl

REFERENCES

(1) Zaumseil, J.; Sirringhaus, H. Electron and Ambipolar Transport in Organic Field-Effect Transistors. *Chem. Rev.* **2007**, *107*, 1296−1323.

(2) Shim, H.; Kumar, A.; Cho, H.; Yang, D.; Palai, A. K.; Pyo, S. Laterally-Stacked, Solution-Processed Organic Microcrystal with Ambipolar Charge Transport Behavior. *ACS Appl. Mater. Interfaces* **2014**, *6*, 17804−17814.

(3) Zhao, Y.; Guo, Y.; Liu, Y. Recent Advances in n-Type and Ambipolar Organic Field-Effect Transistors. *Adv. Mater.* **2013**, *25*, 5372−5391.

(4) Ahn, K.; Kim, J. B.; Park, H.; Kim, H.; Lee, M. H.; Kim, B. J.; Cho, J. H.; Kang, M. S.; Lee, D. R. Enhancing Crystallinity of C_{60} Layer by Thickness-Control of Underneath Pentacene Layer for High Mobility C_{60}/Pentacene Ambipolar Transistors. *Appl. Phys. Lett.* **2013**, *102*, 043306.

(5) Wang, J.; Wang, H.; Yan, X.; Huang, H.; Jin, D.; Shi, J.; Tang, Y.; Yan, D. Heterojunction Ambipolar Organic Transistors Fabricated by a Two-Step Vacuum-Deposition Process. *Adv. Funct. Mater.* **2006**, *16*, 824−830.

(6) To the best of our knowledge, ambipolar organic field effect transistors composed of solution-processed p-n semiconductor bilayers were only documented once with single-crystalline p−n junctions. See: Fan, C.; Zoombelt, A. P.; Jiang, H.; Fu, W.; Wu, J.; Yuan, W.; Wang, Y.; Li, H.; Chen, H.; Bao, Z. Solution-Grown Organic Single-Crystalline p-n Junctions with Ambipolar Charge Transport. *Adv. Mater.* **2013**, *25*, 5762−5766.

(7) Li, H.; Fan, C.; Fu, W.; Xin, H. L.; Chen, H. Solution-Grown Organic Single-Crystalline Donor-Acceptor Heterojunctions for Photovoltaics. *Angew. Chem., Int. Ed.* **2015**, *54*, 956−960.

(8) Meijer, E. J.; Leeuw, D. M. D.; Setayesh, S.; Veenendaal, E. V.; Huisma, B.-H.; Blom, P. W. M.; Hummelen, J. C.; Scherf, U.; Klapwijk, T. M. Solution-Processed Ambipolar Organic Field-Effect Transistors and Inverters. *Nat. Mater.* **2003**, *2*, 678−682.

(9) Yang, S. H.; Cho, M. Y.; Jo, S. G.; Jung, J. S.; Jung, K. H.; Bae, S. Y.; Choi, D. H.; Kim, S.; Joo, J. Photoresponsive Ambipolar Transport Characteristics of Organic Thin Film Transistors Using Soluble HB-ant-THT and PCBM Composites. *Synth. Met.* **2012**, *162*, 332−336.

(10) Abbas, M.; Tekin, N. Balanced Charge Carrier Mobilities in Bulk Heterojunction Organic Solar Cells. *Appl. Phys. Lett.* **2012**, *101*, 073302.

(11) Puniredd, S. R.; Kiersnowski, A.; Battagliarin, G.; Zajączkowski, W.; Wong, W. W. H.; Kirby, N.; Müllen, K.; Pisula, W. Polythiophene−Perylene Diimide Heterojunction Field-Effect Transistors. *J. Mater. Chem. C* **2013**, *1*, 2433−2440.

DOI: 10.1021/acsami.5b01172
ACS Appl. Mater. Interfaces XXXX, XXX, XXX−XXX

(12) Cheng, S.-S.; Huang, P.-Y.; Ramesh, M.; Chang, H.-C.; Chen, L.-M.; Yeh, C.-M.; Fung, C.-L.; Wu, M.-C.; Liu, C.-C.; Kim, C.; Lin, H.-C.; Chen, M.-C.; Chu, C.-W. Solution-Processed Small-Molecule Bulk Heterojunction Ambipolar Transistors. *Adv. Funct. Mater.* **2014**, *24*, 2057−2063.
(13) Lombardo, C.; Dodabalapur, A. Nongeminate Carrier Recombination Rates in Organic Solar Cells. *Appl. Phys. Lett.* **2010**, *97*, 233302.
(14) Zhang, Y.; Liu, J.; Nguyen, T.-Q. Photoresponse of Donor/Acceptor Blends in Organic Transistors: A Tool for Understanding Field-Assisted Charge Separation in Small Molecule Bulk Heterojunction Solar Cells. *ACS Appl. Mater. Interfaces* **2013**, *5*, 2347−2353.
(15) Hasegawa, T.; Mattenberger, K.; Takeya, J.; Batlogg, B. Ambipolar Field-Effect Carrier Injections in Organic Mott Insulators. *Phys. Rev. B* **2004**, *69*, 245115.
(16) Sakai, M.; Sakuma, H.; Ito, Y.; Saito, A.; Nakamura, M.; Kudo, K. Ambipolar Field-Effect Transistor Characteristics of (BEDT-TTF)(TCNQ) Crystals and Metal-Like Conduction Induced by a Gate Electric Field. *Phys. Rev. B* **2007**, *76*, 045111.
(17) Zhang, J.; Geng, H.; Virk, T. S.; Zhao, Y.; Tan, J.; Di, C.; Xu, W.; Singh, K.; Hu, W.; Shuai, Z.; Liu, Y.; Zhu, D. Sulfur-Bridged Annulene-TCNQ Co-Crystal: A Self-Assembled "Molecular Level Heterojunction" with Air Stable Ambipolar Charge Transport Behavior. *Adv. Mater.* **2012**, *24*, 2603−2607.
(18) Park, S. K.; Varghese, S.; Kim, J. H.; Yoon, S.-J.; Kwon, O. K.; An, B.-K.; Gierschner, J.; Park, S. Y. Tailor-Made Highly Luminescent and Ambipolar Transporting Organic Mixed Stacked Charge-Transfer Crystals: An Isometric Donor−Acceptor Approach. *J. Am. Chem. Soc.* **2013**, *135*, 4757−4764.
(19) Black, H. T.; Perepichka, D. F. Crystal Engineering of Dual Channel p/n Organic Semiconductors by Complementary Hydrogen Bonding. *Angew. Chem., Int. Ed.* **2014**, *53*, 2138−2142.
(20) Zhang, J.; Tan, J.; Ma, Z.; Xu, W.; Zhao, G.; Geng, H.; Di, C.; Hu, W.; Shuai, Z.; Singh, K.; Zhu, D. Fullerene/Sulfur-Bridged Annulene Cocrystals: Two-Dimensional Segregated Heterojunctions with Ambipolar Transport Properties and Photoresponsivity. *J. Am. Chem. Soc.* **2013**, *135*, 558−561.
(21) For the mixture to be considered a solid solution, the crystal structure of the solvent must remain essentially unchanged upon the addition of the solute(s) and the whole mixture must remain as a single homogeneous phase. See: Steed, J. W.; Atwood, J. L. *Supramolecular Chemistry*, 2nd ed.; Wiley: New York, 2009.
(22) Hinderhofer, A.; Schreiber, F. Organic-Organic Heterostructures: Concepts and Applications. *ChemPhysChem* **2012**, *13*, 628−643.
(23) Nénon, S.; Kanehira, D.; Yoshimoto, N.; Fages, F.; Videlot-Ackermann, C. Ambipolar Organic Field-Effect Transistors Based on CuPc and F_{16}CuPc: Impact of the Fine Microstructure at Organic-Organic Interface. *Synth. Met.* **2011**, *161*, 1915−1920.
(24) Xu, X.; Shan, B.; Kalytchuk, S.; Xie, M.; Yang, S.; Liu, D.; Kershaw, S. V.; Miao, Q. Synthesis, Solution-Processed Thin Film Transistors and Solid Solutions of Silylethynylated Diazatetracenes. *Chem. Commun.* **2014**, *50*, 12828−12831.
(25) Miao, S.; Appleton, A. L.; Berger, N.; Barlow, S.; Marder, S. R.; Hardcastle, K. I.; Bunz, U. H. F. 6,13-Diethynyl-5,7,12,14-Tetraazapentacene. *Chem.—Eur. J.* **2009**, *15*, 4990−4993.
(26) Liang, Z.; Tang, Q.; Xu, J.; Miao, Q. Soluble and Stable N -Heteropentacenes with High Field-Effect Mobility. *Adv. Mater.* **2011**, *23*, 1535−1539.
(27) Liu, D.; Xu, X.; Su, Y.; He, Z.; Xu, J.; Miao, Q. Self-Assembled Monolayers of Phosphonic Acids with Enhanced Surface Energy for High-Performance Solution-Processed N-Channel Organic Thin-Film Transistors. *Angew. Chem., Int. Ed.* **2013**, *52*, 6222−6227.
(28) Liu, D.; He, Z.; Su, Y.; Diao, Y.; Mannsfeld, S. C. B.; Bao, Z.; Xu, J.; Miao, Q. Self-Assembled Monolayers of Cyclohexyl-Terminated Phosphonic Acids as a General Dielectric Surface for High-Performance Organic Thin-Film Transistors. *Adv. Mater.* **2014**, *26*, 7190−7196.
(29) Anthony, J. E.; Brooks, J. S.; Eaton, D. L.; Parkin, S. R. Functionalized Pentacene: Improved Electronic Properties from Control of Solid-State Order. *J. Am. Chem. Soc.* **2001**, *123*, 9482−9483.
(30) Sakanoue, T.; Sirringhaus, H. Band-Like Temperature Dependence of Mobility in a Solution-Processed Organic Semiconductor. *Nat. Mater.* **2010**, *9*, 736−740.
(31) Park, S. K.; Jackson, T. N.; Anthony, J. E.; Mourey, D. A. High Mobility Solution Processed 6,13-bis(Triisopropyl-Silylethynyl) Pentacene Organic Thin Film Transistors. *Appl. Phys. Lett.* **2007**, *91*, 063514.
(32) Giri, G.; Verploegen, E.; Mannsfeld, S. C. B.; Atahan-Evrenk, S.; Kim, D. H.; Lee, S. Y.; Becerril, H. A.; Aspuru-Guzik, A.; Toney, M. F.; Bao, Z. Tuning Charge Transport in Solution-Sheared Organic Semiconductors Using Lattice Strain. *Nature* **2011**, *480*, 504−508.
(33) Yang, X.; Liu, D.; Miao, Q. Heptagon-Embedded Pentacene: Synthesis, Structures, and Thin-Film Transistors of Dibenzo[d,d′]-benzo[1,2-a:4,5-a′]dicycloheptenes. *Angew. Chem., Int. Ed.* **2014**, *53*, 6786−6790.
(34) Lucia, E. A.; Verderame, F. D. Spectra of Polycrystalline Phthalocyanines in the Visible Region. *J. Chem. Phys.* **1968**, *48*, 2674−2681.
(35) Ding, Y.; Simonyan, M.; Yonehara, Y.; Uruichi, M.; Yakushi, K. Preparation and Characterization of Phthalocyanine-Based Organic Alloy $Co_xNi_{1-x}Pc(AsF_6)_{0.5}$ ($0 \leq x \leq 1$). *J. Mater. Chem.* **2001**, *11*, 1469−1475.
(36) For an example of single crystals of solid solution, see: Li, J.; Takaishi, S.; Fujinuma, N.; Endo, K.; Yamashita, M.; Matsuzaki, H.; Okamoto, H.; Sawabe, K.; Takenobu, T.; Iwasa, Y. Enhancement of Luminescence Intensity in TMPY/Perylene Co-Single Crystals. *J. Mater. Chem.* **2011**, *21*, 17662−17666.
(37) Su, Y.; Wang, C.; Xie, W.; Xie, F.; Chen, J.; Zhao, N.; Xu, J. Low-Voltage Organic Field-Effect Transistors (OFETs) with Solution-Processed Metal-Oxide as Gate Dielectric. *ACS Appl. Mater. Interfaces* **2011**, *3*, 4662−4667.
(38) Nonnenmacher, M.; O'Boyle, M.; Wichramasinghe, H. K. *Ultramicroscopy* **1992**, *42*−*44*, 268−273.
(39) Hoppe, H.; Glatzel, T.; Niggemann, M.; Hinsch, A.; Lux-Steiner, M. C.; Sariciftci, N. S. Kelvin Probe Force Microscopy Study on Conjugated Polymer/Fullerene Bulk Heterojunction Organic Solar Cell. *Nano Lett.* **2005**, *5*, 269−274.
(40) Melitz, W.; Shen, J.; Kummel, A. C.; Lee, S. Kelvin Probe Force Microscopy and Its Application. *Surf. Sci. Rep.* **2011**, *66*, 1−27.
(41) Palermo, V.; Otten, M. B. J.; Liscio, A.; Schwartz, E.; de Witte, P. A. J.; Castriciano, M. A.; Wienk, M. M.; Nolde, F.; De Luca, G.; Cornelissen, J. J. L. M.; Janssen, R. A. J.; Müllen, K.; Rowan, A. E.; Nolte, R. J. M.; Samorì, P. The Relationship between Nanoscale Architecture and Function in Photovoltaic Multichromophoric Arrays as Visualized by Kelvin Probe Force Microscopy. *J. Am. Chem. Soc.* **2008**, *130*, 14605−14614.
(42) Liscio, A.; De Luca, G.; Nolde, F.; Palermo, V.; Müllen, K.; Samorì, P. Photovoltaic Charge Generation Visualized at the Nanoscale: A Proof of Principle. *J. Am. Chem. Soc.* **2008**, *130*, 780−781.
(43) De Sio, A.; Madena, T.; Huber, R.; Parisi, J.; Neyshtadt, S.; Deschler, F.; Da Como, E.; Esposito, S.; von Hauff, E. Solvent Additives for Tuning the Photovoltaic Properties of Polymer−Fullerene Solar Cells. *Solar Energy Mater. Solar Cells* **2011**, *95*, 3536−3542.
(44) Akaike, K.; Kanai, K.; Ouchi, Y.; Seki, K. Impact of Ground-State Charge Transfer and Polarization Energy Change on Energy Band Offsets at Donor/Acceptor Interface in Organic Photovoltaics. *Adv. Funct. Mater.* **2010**, *20*, 715−721.
(45) Gao, C. H.; Zhu, X. Z.; Zhang, L.; Zhou, D. Y.; Wang, Z. K.; Liao, L. S. Comparative Studies on the Inorganic and Organic p-Type Dopants in Organic Light-Emitting Diodes with Enhanced Hole Injection. *Appl. Phys. Lett.* **2013**, *102*, 153301.
(46) Matsushima, T.; Jin, G. H.; Kanai, Y.; Yokota, T.; Kitada, S.; Kishi, T.; Murata, H. Interfacial Charge Transfer and Charge

DOI: 10.1021/acsami.5b01172
ACS Appl. Mater. Interfaces XXXX, XXX, XXX−XXX

Generation in Organic Electronic Devices. *Org. Electron.* **2011**, *12*, 520−528.
(47) Matsushima, T.; Murata, H. Observation of Space-Charge-Limited Current due to Charge Generation at Interface of Molybdenum Dioxide and Organic Layer. *Appl. Phys. Lett.* **2009**, *95*, 203306.
(48) Xue, G.; Fan. C.; Wu. J.; liu, S.; liu, Y.; Chen, H.; Xin, H. L.; Li, H. Ambipolar Charge Transport of TIPS-Pentacene Single-Crystals Grown from Non-Polar Solvents, *Mater. Horiz.* **2015**, DOI: 10.1039/C4MH00211C.
(49) Zhang, Y.; Dong, H.; Tang, Q.; Ferdous, S.; Liu, F.; Mannsfeld, S. C. B.; Hu, W.; Briseno, A. L. Organic Single-Crystalline p-n Junction Nanoribbons. *J. Am. Chem. Soc.* **2010**, *132*, 11580−11584.
(50) Kim, J. H.; Yun, S. W.; An, B.-K.; Han, Y. D.; Yoon, S.-J.; Joo, J.; Park, S. Y. Remarkable Mobility Increase and Threshold Voltage Reduction in Organic Field-Effect Transistors by Overlaying Discontinuous Nano-Patches of Charge-Transfer Doping Layer on Top of Semiconducting Film. *Adv. Mater.* **2013**, *25*, 719−724.
(51) The red light was emitted by a LED lamp, whose emission spectrum is shown in Figure S3 of the Supporting Information. The intensity of this red light was calibrated with a Newport model 1916-C/-R hand-held optical power meter.

DOI: 10.1021/acsami.5b01172
ACS Appl. Mater. Interfaces XXXX, XXX, XXX−XXX